
RACAM: ENHANCING DRAM WITH REUSE-AWARE COMPUTATION AND AUTOMATED MAPPING FOR ML INFERENCE

Siyuan Ma

Department of Electrical and Computer Engineering
 University of Texas at Austin
 Austin, TX 78712
 siyuan.ma@utexas.edu

Jiajun Hu

School of Computing and Augmented Intelligence
 Arizona State University
 Tempe, AZ 85281
 jiajunh5@asu.edu

Jeeho Ryoo

Olsen College of Engineering and Science
 Fairleigh Dickinson University
 Vancouver
 j.ryoo@fd.edu

Aman Arora

School of Computing and Augmented Intelligence
 Arizona State University
 Tempe, AZ 85281
 aman.kbm@asu.edu

Lizy Kurian John

Department of Electrical and Computer Engineering
 University of Texas at Austin
 Austin, TX 78712
 ljohn@ece.utexas.edu

December 11, 2025

ABSTRACT

In-DRAM Processing-In-Memory (DRAM-PIM) has emerged as a promising approach to accelerate memory-intensive workloads by mitigating data transfer overhead between DRAM and the host processor. Bit-serial DRAM-PIM architectures, further enhance efficiency by supporting runtime variable data precision, which is critical for emerging workloads, such as large language model (LLM) inference. However, existing works still have major limitations: lack of data reuse, significant amounts of redundant data transfer, and insufficient support for workload mapping. To address these issues, we propose *RACAM*, the first in-DRAM bit-serial architecture which uses dedicated locality buffers, bit-serial PEs, popcount reduction units and broadcast units to enable data reuse and alleviate redundant data transfers. Furthermore, a workload mapping mechanism is proposed to fully explore the massive parallelism of DRAM architecture and identify the best mapping scheme of a given workload. We evaluate *RACAM* against GPUs and the state-of-the-art, in-DRAM PIM system, Proteus, across end-to-end LLM inferences. *RACAM* achieves $9\times$ to $102\times$ speedup over GPUs and $233\times$ higher performance per mm^2 compared to Proteus in case of GPT3.

1 Introduction

As AI models continue to grow in scale and complexity, the demand for sustained data movement between memory and compute units has increased substantially. In large language models (LLMs), whose dominant operators are general matrix–matrix and matrix–vector multiplications (GEMM/GEMV), performance is fundamentally constrained by memory bandwidth rather than by the raw compute capability of GPU compute cores. Even with large GPU clusters equipped with high-bandwidth memory, LLM throughput fails to scale proportionally because the memory subsystem cannot supply data at the rate required by these operators, making memory the primary performance and energy bottleneck in contemporary LLM workloads [3, 12, 64]. In response, major memory vendors including Samsung, SK

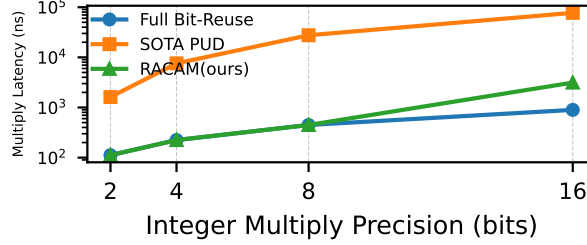


Figure 1: Integer Multiplication Latency

Hynix, and Micron are developing processing-in-memory (PIM) and processing-near-memory (PNM) architectures to more efficiently accelerate memory-bound workloads. [10, 23, 45, 82].

Beyond limitations imposed by memory bandwidth, precision flexibility has become an increasingly important requirement for modern workloads such as DNNs and LLMs [29, 53, 71, 87], which exhibit varying numerical sensitivity across layers and therefore benefit from architectures that adapt numerical precision to each layer’s error tolerance and algorithmic requirements. To support such variability, prior work has explored several precision-scalable PIM mechanisms including bit-serial, bit-sliced, and mixed-precision designs. Among these options, bit-serial PIM is particularly appealing due to its natural scaling with DRAM row parallelism and ability to adjust effective precision through serialization. Recent Processing-Using-DRAM (PUD) systems [14, 19, 20, 59] demonstrate that DRAM arrays can execute massively parallel bit-serial logic operations by exploiting charge sharing and sense-amplifier behavior within largely standard DRAM ACT/PRE command sequences, enabling high area efficiency and improved performance-per-mm² for memory-bound workloads.

Existing PUD systems, however, exhibit long multiplication latencies because all multiplicand bits must be accessed for every bit of the multiplier, resulting in $O(n^2)$ quadratic scaling latencies for an n -bit integer multiply [14]. In DRAM-based bit-serial logic, each operand-bit access typically incurs a row activation and precharge, so repeatedly revisiting the same operand bits generates a large number of ACT–PRE cycles. This inefficiency arises from the lack of bit-level locality in current PUD data mappings as operand bits are not positioned to allow reuse, forcing the system to re-read the same bits for every partial product. Fig. 1 quantifies this effect. The orange curve (“SOTA PUD”) shows a design with no bit reuse, where multiplication latency grows steeply because every multiplicand bit is fetched independently for each multiplier bit. The blue curve represents an idealized design with full bit reuse, where operand bits are accessed once and reused across all partial products, yielding far lower latency growth. Overall, the figure highlights that excessive row activations caused by bit-level non-locality are the dominant contributor to multiplication latency in existing PUD systems.

Another challenge in PUD systems is the cost of transferring dynamic data across the DRAM hierarchy. While DRAM PIMs and PUDs reduce data movement to central processing units, there is need for significant data transfer in intermediate steps. While static operands (such as weights) can be pre-duplicated offline in whatever pattern that maximizes parallelism, dynamic operands such as activations, intermediate data, or kernel inputs must be replicated at runtime to columns or bank that participates in parallel computation. For example, if an input matrix tile A must be available in all banks to enable parallel partial-product generation, prior PUD systems such as ComputeDRAM and SIMDRAm rely on the host processor to explicitly write A into each bank, incurring roughly $\# \text{Banks} \times \text{Bytes}_A$ of data movement across the memory channel [19, 20]. Although DRAM provides high internal bandwidth, this replication is performed over the off-chip CPU–DRAM interface, so the overhead is again dominated by limited channel bandwidth and increased energy per transferred byte. In contrast, providing an internal DRAM-supported broadcast pathway would reduce the required off-chip transfer to only Bytes_A , allowing the duplication to occur within DRAM’s high-bandwidth internal fabric and significantly lowering data-movement overhead.

In addition, the design of systematic workload-to-DRAM mappings remains insufficiently generalized in prior DRAM-based PIM research. Existing works do incorporate mapping strategies, but they are typically tightly coupled to specific operators, dataflows, or DRAM organizations such as hand-crafted layouts for bit-parallel logic in SIMDRAm and Proteus [14, 20], fixed mapping patterns designed around a particular computation model [23], or heuristic, architecture-specific placement policies as in MIMDRAM [59]. While these approaches enable their respective mechanisms, they do not provide a general mapping framework that exposes the full design space. We envision that the GEMM mapping spaces can be formalized as dimensions mapped to DRAM hierarchical structures, and analytical performance models can be used to automatically search through the entire space and generate the mapping. The mappings explored in

prior work tend to be largely manual, narrow in scope, limiting portability across different DRAM configurations and reducing adaptability to diverse or dynamically changing workload dimensions.

To address these limitations, we propose *RACAM*, a scalable in-DRAM bit-serial PIM architecture that enables high-throughput and reliable computation for AI workloads by jointly improving bit-level reuse, operand locality, data broadcasting, and workload mapping. *RACAM* introduces bit-serial processing elements with locality buffers that significantly reduce redundant ACT-PRE operations by reusing operand bits across partial products. This leads to *RACAM* approaching the ideal behavior in Fig. 1 (shown in green). To minimize host-to-DRAM traffic, *RACAM* integrates an internal broadcast unit that replicates dynamic operands across banks entirely within DRAM’s high-bandwidth fabric, avoiding costly off-chip transfers. In addition, *RACAM* provides a generalized mapping framework that separates mapping decisions from both workload structure and DRAM organization, enabling systematic exploration of the mapping space across diverse DRAM configurations. Together, these architectural components allow *RACAM* to efficiently accelerate end-to-end AI workloads while respecting DRAM reliability constraints and preserving area efficiency.

Specifically, this work makes the following contributions:

- We present *RACAM*, an in-DRAM bit-serial PIM architecture that integrates bit-serial PEs with locality buffers for scalable AI acceleration.
- We reduce redundant row activations by enabling bit-level operand reuse across partial products.
- We introduce an internal DRAM broadcast unit that replicates dynamic operands across banks without host involvement, reducing data transfer overheads.
- We provide a generalized mapping framework that decouples workload structure from DRAM configuration to explore a broad mapping space.

RACAM delivers an average of 90.1x and 15.6x performance improvement over GPUs on two end-to-end inference scenarios with GPT3 and Llama3. Likewise, *RACAM* achieves an average of 46 \times over GPUs for performance/mm² and improvement (geomean) of more than 200 \times over SOTA PIMs with only approximately 4% chip area overhead. The end-to-end throughput improvement over GPUs is significant for decode operations in transformers, but not for prefill operations. Ablation studies showed that, among the added features, locality buffer yields the biggest improvement.

The remainder of this paper is organized as follows. Section 2 introduces the necessary background on DRAM organization, bit-serial computation, and matrix-multiplication tiling and mapping. Section 3 describes the proposed *RACAM* architecture and microarchitectures. Section 4 presents *RACAM*’s mapping and scheduling framework. Sections 5 and 6 detail our evaluation methodology and experimental results. Finally, Sections 7, 8, and 9 provide discussion, related work, and concluding remarks.

2 Background

2.1 DRAM Organization

Fig. 2 illustrates the hierarchical organization of a modern DRAM system. The hierarchy spans from *channels* to *ranks*, *devices*, *banks*, and ultimately *sub-arrays*. [20, 33, 59, 70] Each channel contains multiple ranks; each rank comprises multiple devices; each device is divided into banks; and each bank consists of multiple sub-arrays.

Within an array, data is stored in individual bit cells, where each bit is represented by the charge level of a storage capacitor. Accessing a row begins by asserting the *wordline*, which connects all cells in that row to their corresponding *bitlines*. The small voltage perturbation contributed by each cell is sensed and amplified by the *sense amplifiers*, which restore the full digital value and place the resulting data into the row buffer. Writing data back similarly requires asserting the wordline; the sense amplifiers then drive the bitlines to charge or discharge the capacitors according to the stored value.

2.2 Bit-serial Computation

In contrast to bit-parallel execution, a bit-serial scheme processes one bit of each operand per cycle rather than the full-precision value. Bit-serial computation is typically implemented in a SIMD manner and can offer higher effective throughput than bit-parallel designs, and supports runtime variable data precisions. To support bit-serial operations in DRAM, data must be stored in a vertically transposed layout, aligning bits of the same significance across DRAM subarray columns. This layout is usually generated by a transpose unit. [14, 20, 55, 59]

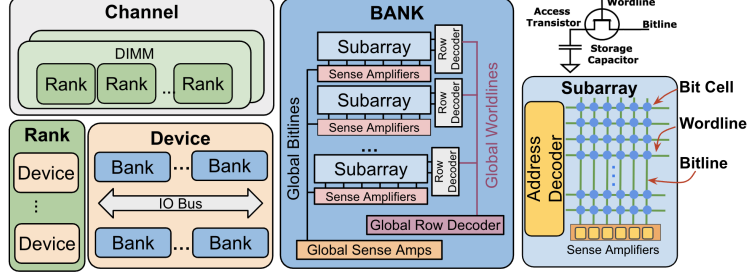


Figure 2: DRAM organization overview.

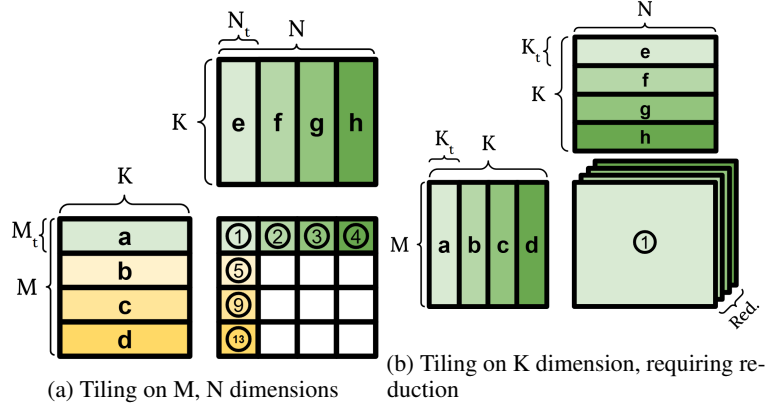


Figure 3: Tiling of Matrix Multiplication

Static data such as model weights can be pre-transposed and written to DRAM offline as a one-time preprocessing step. [14, 20, 59, 70] For a more detailed discussion of bit-serial arithmetic and its use in DRAM-PIM architectures, we refer readers to prior works [4, 20, 59].

2.3 Tiling & Mapping of Matrix Multiplication

Fig. 3 illustrates representative tiling strategies for matrix multiplication, where tiling choices dictate the amount of data movement, the degree of data duplication, and the level of parallelism exploitable by the system. Each processor computes one tile (shown in different colors) in parallel with others.

Tiling along the M or N dimensions introduces **data duplication**. In Fig. 3a, the M and N dimensions are partitioned into tiles of size M_t and N_t , respectively. Computing the four output tiles (1–4) requires the input tiles (a, e) , (a, f) , (a, g) , and (a, h) , implying that tile a must be replicated across four processors when each output tile is assigned to a single processor. Similarly, tile e is duplicated across processors #1, #5, #9, and #13.

Tiling along the K dimension, in contrast, creates **partial outputs** and introduces **reduction**. In Fig. 3b, the K dimension is partitioned into K_t , and each processor produces a partial sum of one output tile. A reduction across the four processors is then required to accumulate these partial results into the final output matrix. Tiling across M , N , and K can be combined to explore a larger space of parallelization and data-movement trade-offs.

In the context of in-DRAM processing, DRAM's hierarchical organization naturally corresponds to multiple levels of parallel processors. For example, four ranks can be viewed as coarse-grained processors, while the sixteen banks within each rank behave as fine-grained parallel sub-processors. Mapping matrix tiles to this hierarchy is more involved, as each hierarchy level can be paired with a distinct tiling dimension. The sensitivity of tiling choices and hierarchy-aware mappings is further examined in Section 4.

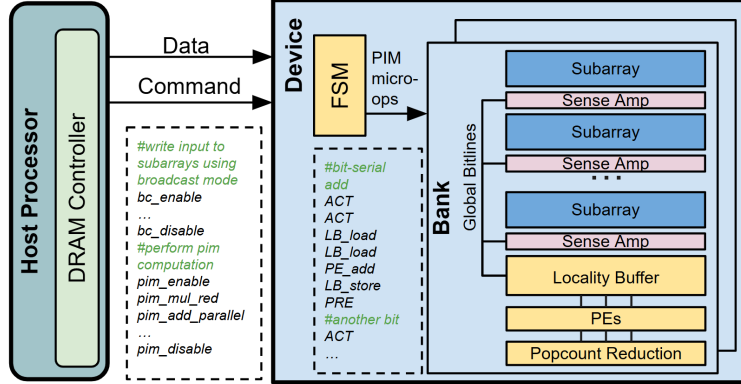
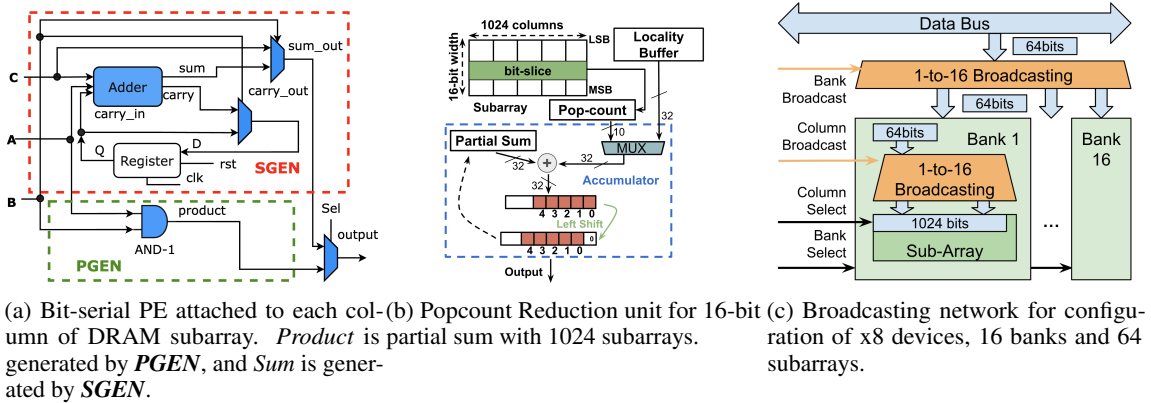


Figure 4: RACAM system overview. Added peripherals are colored in yellow; broadcasting units are not shown.



(a) Bit-serial PE attached to each column of DRAM subarray. *Product* is partial sum with 1024 subarrays. *generated by PGEN*, and *Sum* is generated by *SGEN*. (b) Popcount Reduction unit for 16-bit configuration of x8 devices, 16 banks and 64 subarrays.

Figure 5: Added peripheral units to RACAM architecture

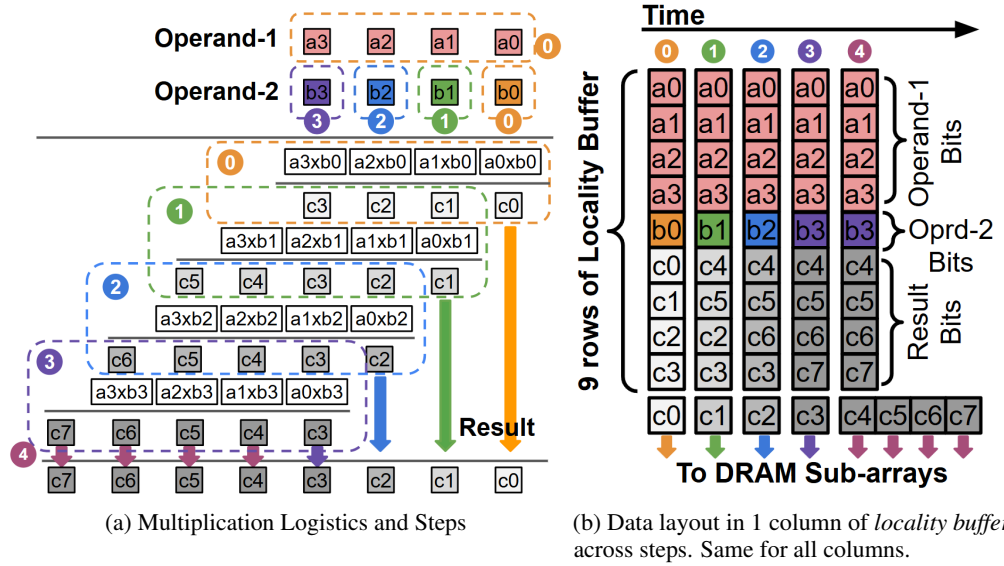


Figure 6: Example of int4 bit-serial multiplication.

Table 1: Extended PIM Commands and Their Instruction Encodings.

Instruction	Opcode Field	Operand Fields	Control Field	Description
pim_enable	000010	–	–	Enables the PIM operating mode through a Mode Register Set (MRS) write
pim_disable	000011	–	–	Disables PIM mode and restores normal DRAM command decoding
broadcast_enable	000000	–	bank_bc, col_bc	Enables broadcast write mode of bank or column
broadcast_disable	000001	–	–	Disables broadcast mode
pim_add	010000	R _{dst} , R _{src1} , R _{src2}	prec[3:0]	Performs bit-serial addition of operands R _{src1} and R _{src2} , storing the result in R _{dst} .
pim_mul	010001	R _{dst} , R _{src1} , R _{src2}	prec[3:0]	Performs bit-serial multiplication between R _{src1} and R _{src2} , storing product in R _{dst} .
pim_mul_red	010010	R _{dst} , R _{src1} , R _{src2}	prec[3:0]	Performs bit-serial multiplication followed by column-wise popcount reduction.
pim_add_parallel	010011	R _{dst} , R _{src1} , R _{src2}	–	Performs bit-parallel addition using the adder inside the popcount reduction unit.

3 RACAM Architecture

3.1 System Overview

RACAM adds extra units on conventional DRAM and modify the host-DRAM interface to perform efficient reuse-aware in-DRAM processing. As illustrated in Fig. 4, *RACAM* employs 1) extra computing units including locality buffers, bit-serial Processing Elements (PEs) and Popcount Reduction Units at each bank, 2) extra control units - a finite state machine (FSM) at each chip(device), shared by all banks. and 3) extended PIM command interface for the host processor, summarized in Table. 1 . The DRAM controller on host processor is enhanced to send PIM commands through the DRAM command interface. The pim_enable command toggle the DRAM into PIM mode where all incoming PIM commands are decoded by the FSM. For broadcast_enable, broadcast_disable commands, FSM simply configures the Mode Register Set (MRS) and set the data path control signals. For pim_add, pim_mul, pim_mul_red, pim_add_parallel commands, the FSM issues micro-ops to PEs, locality buffer, popcount units and subarrays to perform a corresponding computation. When a PIM kernel is completed, the pim_disable command toggles off the PIM mode and results can be accessed through normal DRAM reads. PIM commands are encoded with previously unused or vendor-reserved command encodings in the DRAM command/address protocol. The operand and control fields are transferred through address bus across multiple cycles depending on field length.

In the following subsections, we describe each type of extra units added upon conventional DRAM.

3.2 Bit-Serial PE

Fig. 5a presents the schematic of the *PE* attached to columns of the *Locality Buffer*. When *B* is positive, the PE performs a 1-bit full add with carry for *C* and *A*. When *B* is negative, the PE routes *C* to *Output* and do not update the carry bit. To perform a bit-serial addition of operands *op1* and *op2*, *B* is set to positive. At each cycle, one bit of *op1* and *op2* are sent to *Result* and *A* , and one bit of *C* is populated at *Output*. For bit-serial multiplication, each cycle the PE update one result bit, depending on the current result bit and corresponding *op1* and *op2* bit values. At each cycle, one bit of *op1* is sent to *A*, one bit of *op2* is sent to *B*, and one bit of result is sent to *C*. If *op2* bit is 0, there is no need to update the result. If *op2* bit is 1, the result bit is updated by adding with the *op1* bit, and the carry bit is updated.

3.3 Locality Buffer & Bit-serial Multiplication

To facilitate bit-level reuse, a *Locality Buffer* is added to each bank to accommodate full operand reuse for bit-serial multiplication. Fig.6 shows an example of int4 bit-serial multiplication using the *locality buffer*.

Fig. 6a illustrates the 5 computing steps of the int4 bit-serial multiplication and 6b shows contents of in locality buffer rows at each step. ① bit#0~3 of operand-1 and bit#0 of operand-2 are loaded to 5 rows of the buffer. Result bit#0~3 are equal to operand-1 If the bit#0 is 1, otherwise 0s. Result bit#0 is then populated back to DRAM sub-array. ② Load bit#1 of operand-2, if that bit is 1, serially update result bits#1~5 by adding to operand-1 bitss#0~3. Bit#1 is immediately populated back to DRAM after updated. ③ Similarly, load operand 2 bit#2 to row buffer, update results bits#2~6 and populate bit#2. ④ Similarly, result bits#3~7 are updated in row buffer and result bit#3 is populated. ⑤ There is no more update on result bits. Bits #4~7 are serially populated.

Using this compute scheme, each operand bit is loaded into the row buffer only once, and each result bit is written to the DRAM array only once. This compute scheme reduces number of DRAM row accesses needed to perform a n-bit multiplication from $O(n^2)$ to $O(n)$ which greatly improves the efficiency of multiplications. To accommodate full reuse of n-bit integer multiplication, $2n + 1$ rows are required. We select 17 rows of locality buffer for full reuse of up to 8-bit integer multiplications.

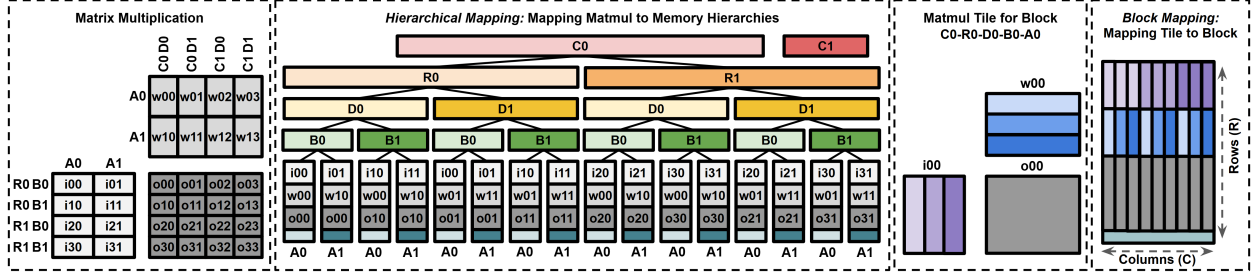


Figure 7: Example of Hierarchical Mapping $\{M: RB, N: CD, K: A\}$ and Block Mapping $\{R : MN, C : K\}$ of Matmul.

RACAM leverages SALP-MASA [41] mechanism to provide highest bandwidth to locality buffer. A row of sub-array is activated before it is accessed and kept activated or precharged while other subarrays are activated. This mechanism saturates the global bitline and provides the highest data bandwidth to locality buffer. To efficiently use this mechanism, rows to be accessed successively in a block are mapped to different sub-arrays to allow overlapped activation.

3.4 Popcount Reduction

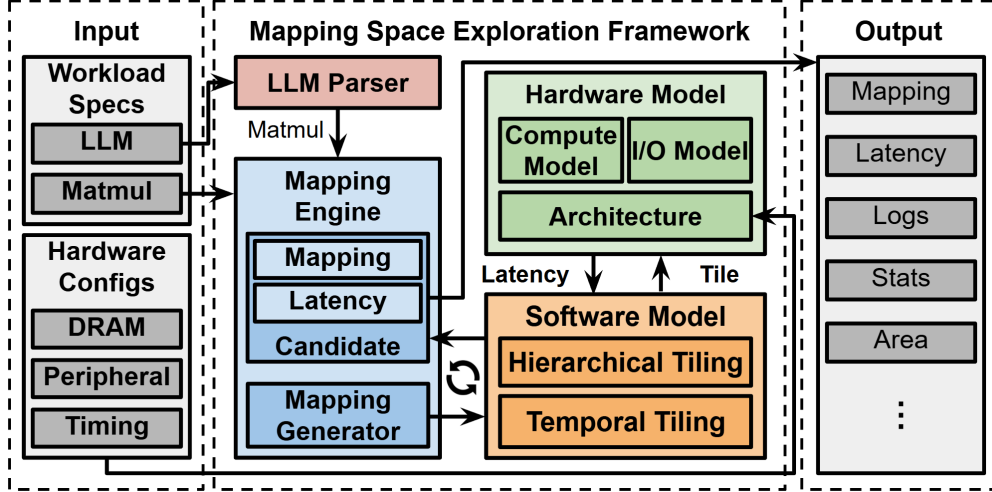
Workloads like matrix-multiplication require cross-column reduction depending on mapping. *RACAM* leverage popcount reduction units added to each bank to perform efficient cross-column reduction. As the vertical data layout allowing only 1 bit of all operands to be accessed at each cycle, a popcount unit is more efficient comparing to a reduction tree. As shown in Fig. 5b, the popcount reduction unit consists of a popcount module and an accumulator, and supports reduction across columns. At each cycle, the popcount module fetches 1 bit of all operand in columns (bit-slice) and calculates number of 1's as a integer. This integer is then shifted and accumulated to the sum. The sum is updated as $sum = sum + \text{popcount}(\text{bitslice}_i) \cdot 2^i$. The `pim_mul_add` command fuses a multiplication with column-wise reduction as they can be efficiently pipelined. The reduction result is written back to DRAM arrays in a horizontal layout to save row activations. In addition, the `pim_add_parallel` leverage the accumulator inside the popcount reduction unit to perform a fast int32 bit-parallel addition, which is useful to add up multiple reduction results.

3.5 Broadcasting Units

To efficiently parallelize workload, some data needs to be broadcasted across one or a few DRAM hierarchies. Although this can be achieved by explicitly write the same data, it introduces redundant data transfers and stresses the DRAM data bus. With hardware broadcasting units, those redundant data writes can be eliminated. As shown in Fig. 5c, broadcasting units are added to the bank and column level to leverage the higher internal bandwidth. At the bank level, each bit of input can be broadcast through a *demux* from the datapath to all banks. When bank broadcasting is enabled, the 64-bit input is broadcast to multiple banks selected by the *Bank Select* signal. Similar to the bank broadcast, at the column level, a *demux* can broadcast each bit to multiple columns of the global row buffer where data is further written back to sub-arrays.

4 Workload Mapping

In order to accomodate flexible workload sizes and efficient exploration of workload mapping, we propose a mapping framework that supports flexible mapping of arbitrary-sized matrix-matrix multiplication (matmul) on arbitrary *RACAM* hardware configuration. In order to efficiently explore parallelism, the mapping framework views the sub-arrays of DRAM as many vertically-divided *Blocks* as the sub-arrays are usually too wide to be mapped naively. A projection from *block* to *sub-array* is performed to determine the physical mapping. For parallelism levels *C* (*Channel*), *R* (*Rank*), *B* (*Bank*), *D* (*Device*), and *A* (*Block*), we define *Hierarchical Mapping* as a projection from each GEMM dimension to certain hierarchies. Within each *block*, we define *Block Mapping* as the projection of *R* (*Row*) and *C* (*Column*) to any GEMM dimensions. For example, Hierarchical Mapping $\{M: RB, N: CD, K: A\}$ means the *M* dimension is hierarchically mapped to *Ranks* and *Banks*, *N* dimension is hierarchically mapped to *Channels* and *Devices*, and *K* dimension is mapped to *Blocks*. Block Mapping $\{R : MN, C : K\}$ means *rows* of a *block* holds the *M* and *N* dimension, while *columns* holds the *K* dimension.

Figure 8: *RACAM* Mapping Framework

4.1 Hierarchical Mapping

Fig. 7 shows an example of mapping a matrix multiplication of size (M, K, N) on DRAM with 2-channel, 2-rank, 2-bank, 2-device, and 2-block. Mapping on channel-1(C1) is not shown due to space limit. The matmul’s M-dimension is hierarchically tiled to *ranks* and *banks*, the K-dimension is tiled to *blocks* and the N-dimension is hierarchically tiled to *channels* and *devices*. The matmul tiles mapped to each block as well as the broadcasting patterns can be inferred by the C,R,D,B,A indices. Note that each input matrix tile is duplicated in 2 devices, indicating need to broadcast. A cross-block reduction can be implied as reduction dimension K is mapped to blocks.

4.2 Block Mapping

Fig. 7 shows an example of block mapping $\{R: M_t N_t, C: K_t\}$ on the right side. After *hierarchical mapping*, each block is assigned a tile, and the *block mapping* further determines the block data layout and computation scheme. In this example, each column of the block contains one slice of matrix $i00$, one slice of matrix $w00$, and computes a partial sum of matrix $o00$. A column-wise reduction is performed across columns. The SIMD multiplications and the column-wise reduction are fused as a `pim_mul_red` instruction for efficient bit-level pipelining.

4.3 Scheduling

After tiling and mapping, if the block is able to hold the entire matmul tile (i.e. with $\{R: MN, C: K\}$, $K_t \leq \#Cols$ and $M_t \times N_t \leq \#rows$), the tile is scheduled to the block without further temporal tiling. In the case that the matmul tile exceeds the size that a block can handle, a further *temporal tiling* is performed to iteratively schedule smaller tiles on a block. For this mapping example, the number of iterations would be $\frac{M}{\sqrt{\#rows}} \times \frac{N}{\sqrt{\#rows}} \times \frac{K}{\#cols}$.

4.4 Mapping Framework

Fig. 8 illustrates the *RACAM* mapping space exploration framework. The framework takes as input the workload specifications (either LLM hyper-parameters or standalone matrix–matrix multiplication shapes) and the hardware configuration, including DRAM organization, peripheral-unit configuration, and timing parameters. The hardware model parameters are summarized in Table 2. For each workload–hardware pair, the framework produces an optimized mapping together with the corresponding end-to-end latency, as well as auxiliary logs, statistics, and area-related reports.

The mapping space exploration framework is composed of an LLM parser, a mapping engine, a software model, and a hardware model. The LLM parser decomposes an input LLM into a sequence of matmul kernels and feeds them to the mapping engine. The mapping engine maintains the current best candidate mapping and its latency. A mapping generator inside the engine enumerates the mapping space, instantiates each mapping, and evaluates it using the software and hardware models, updating the candidate when a lower-latency mapping is found.

The software model applies hierarchical and temporal tiling according to a given mapping, performs scheduling across DRAM hierarchies, and issues per-tile compute and data-movement requests to the hardware model. For each tile, the hardware model returns the computation latency and the I/O latency. The software model accumulates these latencies across temporal tiles; the total kernel latency is the sum of all tile compute latencies and I/O latencies, and is returned to the mapping engine as the objective value of the current mapping.

The hardware model consists of an architectural description, a compute model, and an I/O model. The architecture is parameterized by the input hardware configuration. Given a tile and its mapping, the compute model computes the block-level PIM latency by summing the latencies of all PIM instructions executed on the locality buffers, PEs, and reduction units. The I/O model estimates the latency of interactions with the host CPU across DRAM hierarchies during input broadcasting and output reduction and collection, based on the inferred data layout, the amount of I/O traffic, the effective bandwidth, and the configuration of the broadcasting units. Together, these models enable *RACAM* to explore the full mapping space and identify latency-optimal mappings for each kernel.

Table 2: Hardware Model Parameters

Type	Parameters
DRAM Configuration	#Channels, #Ranks, #Banks, #Devices, #Subarrays, #Rows, #Cols Device Data Width, Frequency global bitline bus width
Peripheral Units Configuration	#PEs, #Locality Buffer Rows, Popcount Reduction Unit Width, Broadcasting Units Width
Timing Parameters	T_{rcd}, T_{rp} PE Latency, Locality Buffer Access Latency, Popcount Reduction Latency

5 Methodology

5.1 Performance Modelling

Similar to previous works’ approach [32, 52, 88], our hardware model is analytical, and hierarchically models the DRAM organization, broadcasting units, processing elements, locality buffers, reduction units and their interconnect. We validate the DRAM timing parameters and bandwidth model with Ramulator [42] and publicly available spec sheets. We implement the added peripheral units in Verilog [78] and obtain their timing parameters using Synopsys Design Compiler [6]. Our LLM Parser is built on top of *LLMCompass* [88].

5.2 Area Estimation

5.2.1 DRAM & locality buffer

We estimate the total DRAM area based on the reported single 16Gb DDR5 die area from *Micron* [77] instead of using DRAM area estimation tools [5, 56] due to the lack of detailed DRAM manufacturing parameters. We assume the DRAM chip storage density (area per bit) remains consistent across different configurations, and the total DRAM chip area is calculated by the product of the unit area per bit and the total storage bits.

The *locality buffer* is modeled similar to aforementioned DRAM area calculation but using the bit-density reported by TSMC 45nm SRAM technology [85]. This SRAM area is later added together with the peripheral logics as the final total added peripheral area.

5.2.2 Peripheral logic

In practice, the periphery logics are fabricated using older, more mature process nodes to ensure greater reliability and thermal stability [31, 72, 74]. Furthermore, DRAM peripheral circuits typically employ fewer interconnect layers than standard CMOS technologies [62].

To evaluate the added peripheral area overhead, we first obtain the synthesis area from *FreePDK 45nm* and *Design Compiler* [1, 75], and scale it down to 14nm, which is one generation older than modern DDR5 manufacturing tech node.

Due the limited access to DRAM and SRAM physical design specs, we estimate the post-synthesis area based on some existing models and projections [35, 36, 73]. There are three major factors affecting the post-synthesis area: placement utilization U , which reflects the area amplified due to place & route; buffer growth factor $\beta \geq 0$, representing the area overhead from clock tree synthesis, timing repair, and resizing; and routing capacity C , which is primarily influenced by the number of metal layers used. The detailed derivation of these parameters is beyond this paper's scope and is omitted for simplicity. With these parameters and synthesis reports, the final post-synthesis area can be calculated.

5.3 Workloads

We evaluate *RACAM* on 4 end-to-end LLMs and their prefill and decode stages. Table 3 summarizes the models' layer, hidden size, number of heads, and quantization precisions. Following the same approach as prior works [26, 47], we choose 2 scenarios for LLM end-to-end inference: *Code Generation* with 1024 prompt tokens and 4096 output tokens as the "prefill heavy" scenario, and *Context Understanding* with 8192 prompt tokens and 256 output tokens as the "decode heavy" scenario. For prefill stage throughput evaluation, we use 1024 as prompt token length. We use batch size=1 for all workloads.

5.4 Evaluated Systems

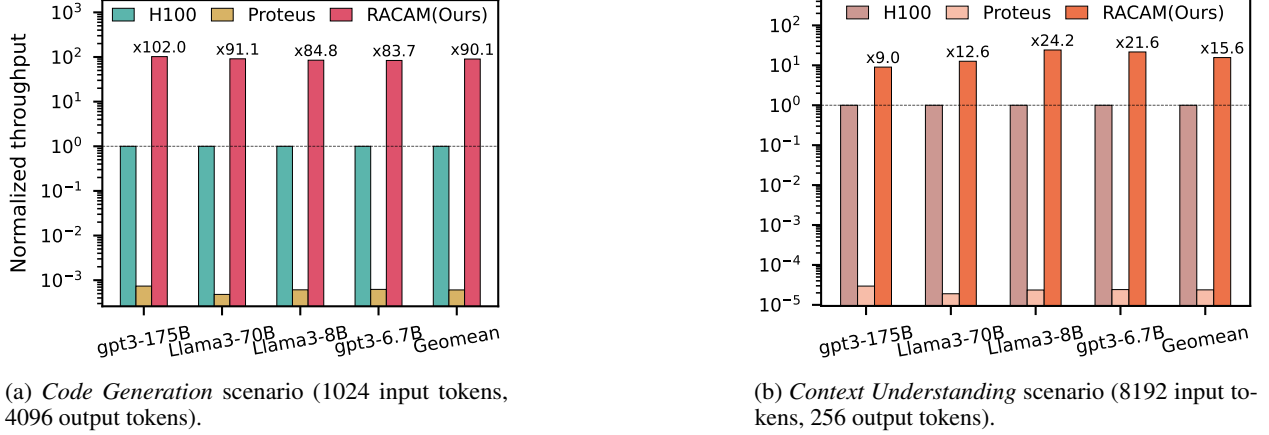
Table 4 shows the systems and configurations we used in evaluation. The H100 system contains an H100 GPU and 512GB host DRAM for data offloading. We use LLMCompass [88], a well-validated simulation framework to evaluate the H100 system latencies. The Proteus system is "consistent" with original paper which contains 1 Channel, 1 Rank and 16 Banks, and we assume 512GB non-PIM host memory for data offloading. We use Proteus' open-source simulator to obtain its latencies. For both H100 and Proteus systems, the added host DRAM is to offload the LLM weights, and we assume zero offloading for those systems. The *RACAM* system configures all 1024GB host memory to PIM-enabled memory, and is evaluated using our open-source simulation framework.

Table 3: Evaluated LLM workloads

Model	Layers	Hidden Size	Heads	Quantization
GPT-3 6.7B	32	4096	32	int8
GPT-3 175B	96	12288	96	int8
Llama-3 8B	32	4096	32	int8
Llama-3 70B	80	8192	64	int8

Table 4: System Configurations

System	Configurations	TOPS ¹
H100(PCIE) [58]	528 Tensor Cores, 80GB HBM3 with 3352GBps bw 512GB Offloading Memory ²	1978.9(int8)
Proteus [14]	1 out-of-order core DDR5-5200, 1 Channel, 1 Rank, 16 Banks 512GB Offloading Memory	0.15(int8)
<i>RACAM</i>	8 Channels, 32 Ranks ³ , 16 Banks, 8 Devices, 128 Sub-arrays, 128 rows, 16K columns per sub-array 1024 PEs per Bank 17x1024 Locality Buffer	986.9(int8)



(a) *Code Generation* scenario (1024 input tokens, 4096 output tokens).

(b) *Context Understanding* scenario (8192 input tokens, 256 output tokens).

Figure 9: End-to-end normalized throughput of H100, *Proteus* and *RACAM* in *Code Generation* and *Context Understanding* cases across evaluated gpt and Llama LLM models.

6 Results

In this section, we evaluate *RACAM* performance using several metrics: *end-to-end throughput*, *prefill throughput*, *decode throughput*, and *performance per mm²*. We compare *RACAM* against the NVIDIA H100 GPU and *Proteus* (Section 6.1). We then conduct an architecture ablation study (Section 6.2) and a sensitivity analysis (Section 6.3) to further characterize the sources of performance improvement and identify key design trade-offs.

6.1 Performance

The normalized end-to-end LLM throughput (also referred to as *request throughput* [44]) of H100, *Proteus*, and *RACAM* is shown in Fig. 9. *RACAM* delivers **90.1x** and **15.6x** higher geometric-mean throughput than H100 on the *Code Generation* and *Context Understanding* scenarios, respectively, while *Proteus* underperforms H100 by orders of magnitude.

Fig. 10 presents the standalone prefill and decode throughput of LLM inference. Although prefill is widely regarded as a compute-bound phase—where conventional PIM architectures typically struggle—*RACAM* still achieves up to **1.9x** speedup over H100. For the memory-bound decode phase, *RACAM* reaches up to **112.0x** speedup due to its high internal bandwidth and the elimination of weight movement from DRAM. While *Proteus* attains relatively better performance during decode than prefill, it still falls short of H100.

Fig. 11 reports the performance per area normalized to H100. We scale H100, *Protues* and *RACAM* area all to 15nm technology. *RACAM* incurs 4% memory chip area overhead, and the total area of peripheral units is 24% of the scaled H100 area⁴. We use 1% to calculate area of added circuitry of *Proteus* as reported [14, 70]. *RACAM* achieves up to **466.8x** and **8.0x** higher performance per area in decode and prefill phases respectively owing to its compact peripheral designs. *Proteus* also exceeds H100 in performance per area, but its improvement is constrained by inefficient bit-serial multiplications without bit-level reuse.

6.2 Architecture Ablation Study

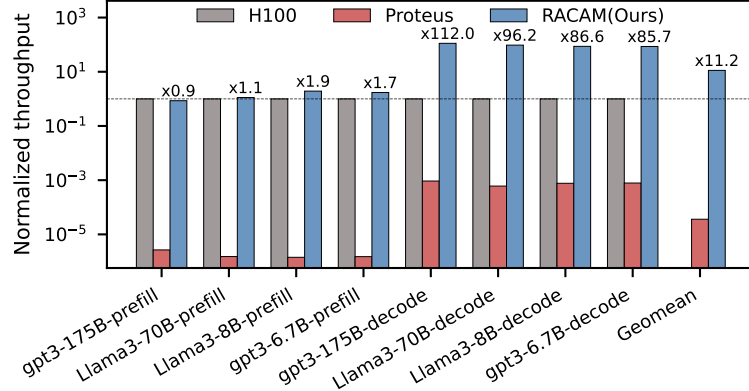
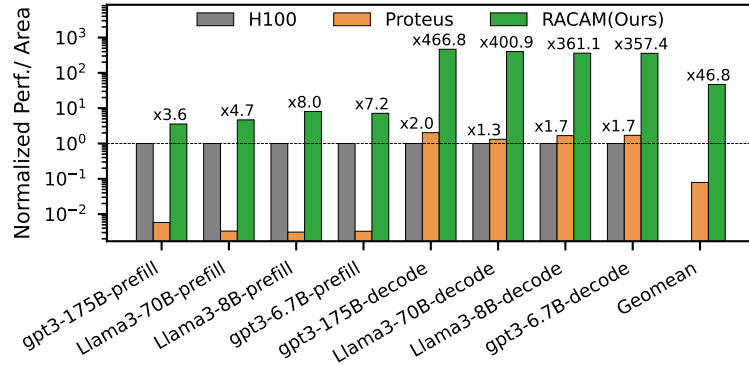
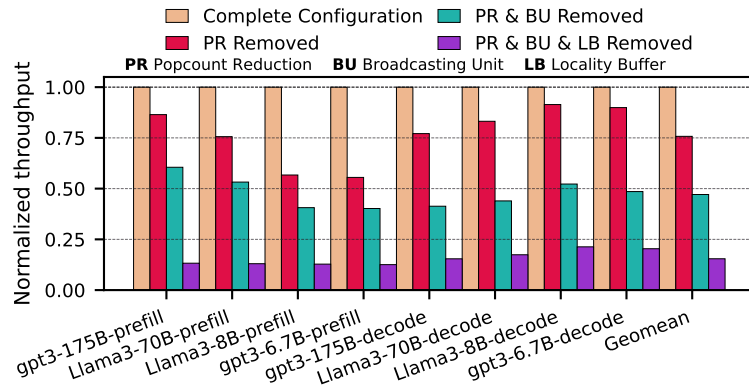
Fig. 12 presents an architectural ablation of *RACAM* across eight LLM workloads, where we progressively disable three key in-DRAM structures: the popcorn reduction (PR) units, the broadcasting units (BU), and the locality buffers (LB). We normalize all results to the complete *RACAM* configuration and report the resulting end-to-end latency degradation. Removing only the PR units already increases prefill latency by 1.2–1.8x, and decode latency by 1.1–1.3x. This

¹H100 TOPS is taken from [58]. We calculate TOPS of *Proteus* and *RACAM* respectively based on their and our simulator.

²NVIDIA reports 512GB LPDDR5X host memory for Grace Hopper Superchip: <https://developer.nvidia.com/blog/nvidia-grace-hopper-superchip-architecture-in-depth/>

³We envision future PIM-enabled memory systems to include more ranks than the JEDEC standard. Rambus already supports up to 16 ranks: <https://www.rambus.com/memory-interface-chips/ddr5-dimm-chipset/ddr5-rcd/>, and FB-DIMM, LR-DIMM [21] effectively increase rank count to 64.

⁴We calculate the H100 area as die + HBM, where HBM is flattened to 1 layer. Both die and HBM are scaled to 15nm tech node.

Figure 10: Normalized end-to-end throughput of *H100*, *Proteus*, and *RACAM*.Figure 11: Performance per unit area of *Proteus* and *RACAM* both normalized to performance per mm^2 of *H100* GPU.Figure 12: *RACAM* Ablation Study - performance is normalized to configuration with all 3 enhancements (locality buffer, popcount and broadcasting unit).

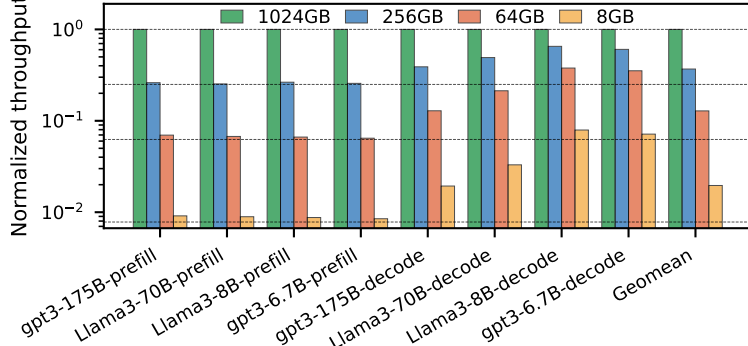


Figure 13: *RACAM* performance sensitivity to system capacity. Horizontal lines represents the normalized capacity ratios (1/8, 1/16, and 1/128), serving as reference for ideal performance scaling.

reflects the cost of exporting partial sums out of the subarray for off-array reduction at host CPU, which increases host data transfer and stresses external bandwidth instead of performing accumulation entirely within the local popcorn reduction units.

When BU is also removed, latency roughly doubles relative to the full design for most decode workloads. Without BU, host CPU must duplicate input across DRAM banks and columns, increasing the host-DRAM data transfers. Removing BU generally has more significant impact on decode workloads, as they are less memory-bound than prefill workloads and more sensitive to data transfer latencies of kernel input.

Finally, eliminating the LB has the largest impact, because it forces all bit-level reuse to go back to the DRAM cell array. Prefill latency increases by about 7.5–8 \times across all models, while decode latency increases by 4.7–6.5 \times . With LB, *RACAM* can keep the multiplicand bit near the PEs and exploit bit-serial reuse at row-buffer granularity; without LB, repeated ACT/PRE and global-bus transfers dominate execution time, shifting the design to strongly memory-bound. Overall, the ablation shows that all three structures—PR, BU, and especially LB—are essential to convert DRAM’s raw internal bandwidth into sustained, high-utilization in-DRAM compute for both prefill and decode.

6.3 Sensitivity Study

6.3.1 PE Number Sensitivity

Fig. 13 presents a sensitivity study on the total number of PEs in the system. We evaluate performance under effective PE counts of 1/4, 1/16, and 1/64 of the baseline by correspondingly reducing the number of channels and ranks. LLM prefill workloads exhibit near-linear degradation that closely follows the PE-reduction reference lines, as they are compute-bound and scale nearly proportionally with available compute resources.

In contrast, LLM decode workloads are far less affected by reductions in PE count and show weak-scaling behavior. Their performance decreases only modestly relative to the reference lines. This behavior arises because (1) decode is primarily memory-bound, and (2) typical decode kernels operate at relatively low PE utilization due to smaller per-token compute footprints, making them less sensitive to compute capacity.

Notably, smaller LLMs experience even less performance loss under reduced PE configurations, since their decoding kernels naturally have lower PE utilization and thus remain more invariant to reductions in compute capability.

6.3.2 Precision Sensitivity

Fig. 14 presents a sensitivity study on workload precision, where data precision is varied from `int8` (baseline) to `int4` and `int2`. Across all workloads, performance increases substantially as precision decreases. Reducing precision from `int8` to `int4` yields approximately 2 \times speedup, and further reducing to `int2` provides 3.5 \times –3.8 \times improvement depending on the workload.

The near-linear scaling arises from the bit-serial compute design with bit-level reuse, which makes latency proportional to operand bit-width for both addition and multiplication. Perfect linear scaling is not achieved due to the fixed latency of the bit-parallel reduction (`pim_add_parallel`), which introduces a constant overhead that becomes more prominent at lower precisions.

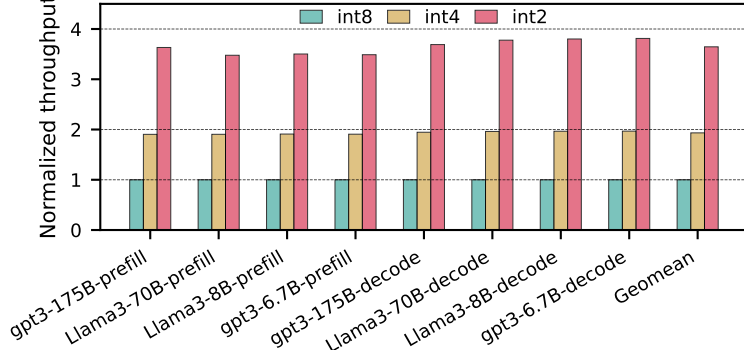


Figure 14: *RACAM* performance sensitivity to workload precision. *RACAM* uses bit-serial scheme, whose latency is ideally linear to data precision.

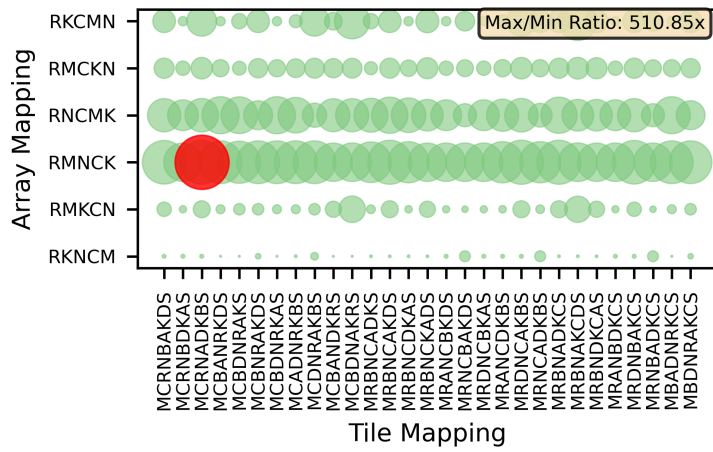


Figure 15: *RACAM* performance sensitivity to mapping strategies on 1024x12288x12288 GEMM. Larger circle means higher performance, red circle has the highest performance.

6.3.3 Mapping sensitivity

Fig. 15 shows the performance sensitivity to workload mapping for a $1024 \times 12288 \times 12288$ GEMM. The scatter plot illustrates that both tile mapping and array mapping exert substantial influence on performance, leading to large variability across mapping strategies (with a maximum-to-minimum ratio of $510.85\times$). Among the array mappings, RNCMK achieves notably higher performance than others, as it can exploit the popcount reduction unit to efficiently perform column-wise reductions. In contrast, spatial mappings exhibit irregular and unpredictable performance trends, underscoring the necessity of systematic design-space exploration rather than relying on manually crafted mapping choices.

6.3.4 GEMM/GEMV Size Sensitivity

Fig. 16 illustrates how GEMM and GEMV latency scales with problem size and how these trends correlate with PE utilization. Across all GEMM configurations, *RACAM* sustains near-ideal scaling despite the rapid growth of arithmetic intensity. For example, increasing the GEMM size from $2048 \times 2048 \times 2048$ to $32768 \times 32768 \times 32768$ enlarges the total compute requirement by $4096\times$, yet latency rises by only $2984.6\times$. This deviation from the capacity-scaled baseline corresponds directly to the increased PE utilization, which increases from 86.3% to 98.0%. Because GEMM kernels achieve full utilization across columns, arrays, banks, channels, and devices (all at 1.0), the improvement stems primarily from two factors: the ability of locality buffers to amortize operand loading as K grows, and the dominance of compute latency over I/O latency at larger scales. For instance, in the largest GEMM, compute latency dominates total latency by $> 98\%$, while I/O contributes only 1.39ms out of 69.9ms.

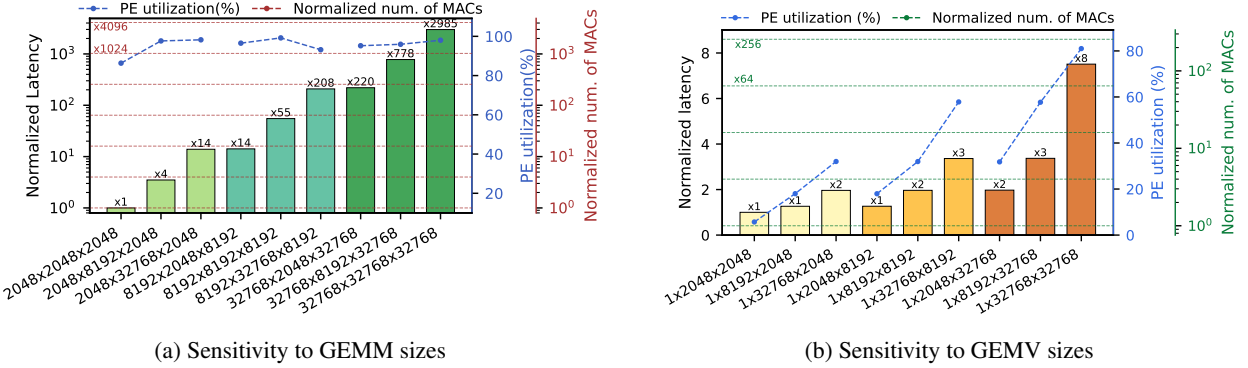


Figure 16: Sensitivity analysis across GEMM and GEMV workloads noted in $M \times K \times N$. Sizes are grouped into 3, M, N are fixed value and only K is changing within each group.

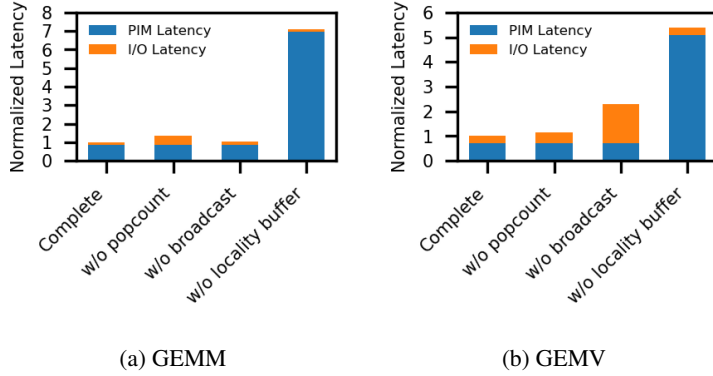


Figure 17: Breakdown of GEMM and GEMV latencies under ablation of hardware as each component is removed.

In contrast, GEMV kernels exhibit a different microarchitectural behavior, as shown in Fig. 16b. GEMV is inherently memory-bound, and thus the achievable PE utilization is much lower (e.g., 7% for $1 \times 2048 \times 2048$ GEMV compared to 82% for large GEMMs). As GEMV size increases, PE utilization improves monotonically due to higher SIMD utilization and arithmetic intensity. This produces sub-linear latency growth: although workload size increases by up to $256 \times$, observed latency increases by only $4 \times$, demonstrating RACAM’s ability to convert additional operand reuse and hierarchical parallelism into effective speedup even for bandwidth-bound workloads.

6.3.5 Latency Breakdown

Fig. 17 illustrates the PIM and I/O latency breakdown of a typical LLM kernel in prefill, GEMM-1x49152x12288, under different scenarios of hardware unit ablation. “PIM Latency” refers to the total latency of PIM compute commands `pim_add`, `pim_mul`, `pim_mul_red`, `pim_add_parallel`. Larger blue portions indicate that the workload is more compute dominated. “I/O Latency” refers to the total latency spend on communication with host, either to layout the kernel input data, fetch the kernel output data or perform host-side reduction. Larger orange portions indicate that the workload is more I/O dominated.

For the “Complete” case without ablation, GEMM latency is clearly compute dominated, corresponding to its compute-bound nature. Although GEMV is intrinsically memory-bound, RACAM leverages broadcasting units, high internal bandwidth, and the ability to store static weight data prior to computation to drastically reduce I/O latency. Removing the popcount adder or broadcasting units both increase I/O latency as more data needs to go through host-dram I/O. Removing the locality buffer drastically increases PIM latency as no bit-level reuse can be exploited, and latency penalties are paid on repeated expensive ACT-PRE operations.

7 Discussion

Reliability: Excessive concurrent row activations pose serious reliability risks in DRAM. Prior work shows that frequent, closely spaced activations accelerate charge leakage and can trigger disturbance errors in nearby rows, exhibiting RowHammer-like behavior [40]. This concern is amplified in PUD architectures, where massively parallel bit-serial operations require dense ACT-PRE sequences across many subarrays.

Unlike CPU-driven access patterns, which are naturally irregular and throttled by cache and instruction dependencies, PUD workloads generate highly regular activation patterns that repeatedly toggle the same wordlines, reducing the time available for cells to restore charge. As concurrent activations increase, vulnerable cells may exceed disturbance thresholds, imposing practical limits on how aggressively bit-level parallelism can be exploited. These challenges highlight the need for PIM architectures that reduce redundant ACT-PRE operations and schedule computation in ways that preserve DRAM integrity.

Moreover, prior studies show that even individual PUD operations are highly sensitive to timing, DRAM chip configuration, and vendor variation [19]. AND/OR operations succeeded reliably on only 1 of 12 evaluated DRAM chips, further emphasizing the importance of using robust digital PEs rather than fragile charge-sharing mechanisms.

Time Taken for Mapping Exploration: Our exhaustive mapping search completes within ~ 1 second for a single GEMV, 2–3 seconds for a single GEMM, and 5–10 seconds for LLM workloads on a 16-core consumer-grade CPU. The search space includes 1,548 candidate mappings for a single GEMM and 192 for GEMV, which has a fixed dimension of 1 require much less tiling and mapping options. The search is very fast as: (1) each evaluation relies on an analytical model and is completed within microseconds, and (2) LLM workloads use consistent GEMM and GEMV shapes across layers, allowing optimal mappings to be reused. Moreover, the search overhead can be pre-paid or amortized. For LLM inference workloads, matrix dimensions vary only with input token length, but because mapping is data-agnostic, mappings for different token lengths can be precomputed or cached at runtime, effectively eliminating repeated search cost.

Integration of Mapping Framework Our mapping framework can be integrated with Front-end / high-level IR such as PyTorch [61], TensorFlow [2], MLIR [46], Halide [66] TVM Relay [9] etc. by annotating PIM-eligible ops and precision. Our proposed framework can act as a mapping pass and codegen backend for lowering IR to PIM instructions, and insert data layout transformations where necessary.

8 Related Work

To the best of our knowledge, *RACAM* is the first bit-serial PIM architecture that enables bit-level data reuse and supports a mapping framework that explores the entire mapping space. Here, we highlight our contributions by comparing with state-of-the-art PIM works shown in table.5.

Processing Using DRAM Prior work [14–16, 18–20, 39, 48, 49, 59, 59, 63, 69, 70, 84, 90] extend in-DRAM mechanisms like row-copy and bulk bitwise operations to implement logic operations using standard DRAM commands [68–70]. These processing-using-DRAM (PUD) systems do not require the integration of additional processing elements (PEs) into DRAM and, in some cases, employ bit-serial schemes to support dynamic bit precision. However, these systems typically offer limited or no data reuse across the system and rely on manually tuned or heuristic-based workload mapping. As a result, existing work [14] shows poor performance on GEMM workloads (2mm, 3mm, gmm from PolyBench [65]) compared to GPUs.

Digital PIM Processing-in-Memory systems with digital PEs are referred to as digital PIM. SRAM-based systems such as NeuralCache [17, 55] and PIMSAB incorporate bit-serial PEs at SRAM arrays to enable computation [17, 55], but still intrinsically limited by DRAM bandwidth. Even DRAM-based systems [8, 23, 25, 30, 50] add near Bank/Subarray PEs, the parallelism are bounded by the DRAM column decoder. Furthermore, the PEs support only fixed precision, limiting the adoption of mixed-precision optimizations. Other systems [22, 34, 51] improve the DRAM search/lookup capability by adding simple logic across memory hierarchies. However, such systems usually support fixed workloads, limiting the scope of broader applicability. *RACAM* adds light-weight bit-serial PEs close to arrays, explores sub-array-level internal bandwidth, and supports broad workloads and flexible precisions.

Mapping Prior works [7, 9, 13, 24, 27, 28, 37, 38, 43, 54, 57, 60, 67, 76, 79–81, 83, 86] present loop-analysis-based mapping techniques or frameworks for ASIC accelerators. However, they do not generalize well to in-DRAM processing architectures due to hierarchical structure and sub-array-aware data layout. Several works [11, 52, 89] propose frameworks to abstract and search the PIM mapping space for loop-based workloads. PIM-DL and ARES use genetic algorithms and OptiPIM use Integer Linear Programming to search over the mapping space. Comparing to those works, *RACAM*’s mapping abstraction limit its scope to the specific mapping space of GEMM, focusing on

Table 5: Comparison of architecture design and mapping methodologies. Assume n bit operands.

Prior Works	Compute Scheme	Row ACTs of n-bit Mult	Broadcast Hardware	Reduction Hardware	Mapping Methodology
Neural Cache	SRAM, bit-serial	–	✓	✗	Manual
PIMSAB	SRAM, bit-serial	–	✓	✓	Heuristics
Newton	DRAM, bit-parallel	$O(n^2)$	✓	✓	Manual
SIMDRAM	DRAM, bit-serial	$O(n^2)$	✗	✗	Manual
MIMDRAM	DRAM, bit-serial	$O(n^2)$	✗	✗	Heuristics
Proteus	DRAM, bit-serial	$O(n^2)$	✗	✗	Manual
<i>RACAM</i> (Ours)	DRAM, bit-serial	$O(n)$	✓	✓	Exhaustive Search

mapping GEMM dimensions to DRAM’s hierarchical architecture. Combined with an analytical performance model, *RACAM* enables searching over the entire mapping space and find the optimal mapping.

9 Conclusion

We introduce *RACAM*, a DRAM based Processing-In-Memory system with bit level reuse and broadcast capabilities. Prior processing in memory architectures struggled with matrix multiplications, while *RACAM* captures locality and significantly accelerates matrix operations and large language models. To achieve full bit level reuse, *RACAM* adds locality buffer to store some bits of operands during integer multiplication. To reduce data reorganization overhead between LLM kernels, *RACAM* adds broadcasting units. To achieve efficient reduction, a common operation in LLM kernels, *RACAM* adds reduction units at each subarray to accelerate column-wise reduction. To efficiently map all matmul kernels of LLM, *RACAM* proposes a mapping framework to automatically search for the optimal mapping strategy for each matmul kernel. We evaluate *RACAM* against the H100 GPU and SOTA DRAM PIM systems, and demonstrate improvements in both performance and performance per area. *RACAM* delivers an average of 90.1x and 15.6x performance improvement over GPUs on two end-to-end inference scenarios with GPT3 and Llama3 workloads. Likewise, *RACAM* achieves an average of 46x over GPUs for performance/mm² and improvement (geomean) of more than 200x over SOTA PIMs with only approximately 4% chip area overhead.

References

- [1] *Synopsys, Inc. Design Compiler Optimization Reference Manual, Version F-2011.09, September 2011.*, 2011.
- [2] M. Abadi, P. Barham, J. Chen, Z. Chen, A. Davis, J. Dean, M. Devin, S. Ghemawat, G. Irving, M. Isard, M. Kudlur, J. Levenberg, R. Monga, S. Moore, D. G. Murray, B. Steiner, P. Tucker, V. Vasudevan, P. Warden, M. Wicke, Y. Yu, and X. Zheng, “Tensorflow: a system for large-scale machine learning,” in *Proceedings of the 12th USENIX Conference on Operating Systems Design and Implementation*, ser. OSDI’16. USA: USENIX Association, 2016, p. 265–283.
- [3] R. Y. Aminabadi, S. Rajbhandari, M. Zhang, A. A. Awan, C. Li, D. Li, E. Zheng, J. Rasley, S. Smith, O. Ruwase, and Y. He, “Deepspeed inference: Enabling efficient inference of transformer models at unprecedented scale,” 2022. [Online]. Available: <https://arxiv.org/abs/2207.00032>
- [4] A. Arora, A. Bhamburkar, A. Borda, T. Anand, R. Sehgal, B. Hanindhito, P.-E. Gaillard, J. Kulkarni, and L. K. John, “Comefa: Deploying compute-in-memory on fpgas for deep learning acceleration,” *ACM Trans. Reconfigurable Technol. Syst.*, vol. 16, no. 3, Jul. 2023. [Online]. Available: <https://doi.org/10.1145/3603504>
- [5] R. Balasubramonian, A. B. Kahng, N. Muralimanohar, A. Shafiee, and V. Srinivas, “Cacti 7: New tools for interconnect exploration in innovative off-chip memories,” *ACM Trans. Archit. Code Optim.*, vol. 14, no. 2, Jun. 2017. [Online]. Available: <https://doi.org/10.1145/3085572>
- [6] H. Bhatnagar, *Advanced ASIC Chip Synthesis: Using Synopsys Design Compiler Physical Compiler and Prime Time*, 2nd ed. USA: Kluwer Academic Publishers, 2002.
- [7] P. Chatarasi, H. Kwon, A. Parashar, M. Pellauer, T. Krishna, and V. Sarkar, “Marvel: A data-centric approach for mapping deep learning operators on spatial accelerators,” *ACM Trans. Archit. Code Optim.*, vol. 19, no. 1, Dec. 2021. [Online]. Available: <https://doi.org/10.1145/3485137>
- [8] L. Chen, D. Lyu, Z. Li, J. Jiang, Q. Wang, Z. Mao, and N. Jing, “Attenpim: Accelerating llm attention with dual-mode gemv in processing-in-memory,” in *2025 62nd ACM/IEEE Design Automation Conference (DAC)*, 2025, pp. 1–7.
- [9] T. Chen, T. Moreau, Z. Jiang, L. Zheng, E. Yan, M. Cowan, H. Shen, L. Wang, Y. Hu, L. Ceze, C. Guestrin, and A. Krishnamurthy, “Tvm: an automated end-to-end optimizing compiler for deep learning,” ser. OSDI’18. USA: USENIX Association, 2018, p. 579–594.
- [10] D. Christ, L. Steiner, M. Jung, and N. Wehn, “Pimsys: A virtual prototype for processing in memory,” in *Proceedings of the International Symposium on Memory Systems*, ser. MEMSYS ’24. New York, NY, USA: Association for Computing Machinery, 2024, p. 26–33. [Online]. Available: <https://doi.org/10.1145/3695794.3695797>
- [11] X. Cui, S. Zheng, T. Jia, L. Ye, and Y. Liang, “Ares: A mapping framework of dnns towards diverse pims with general abstractions,” in *2023 IEEE/ACM International Conference on Computer Aided Design (ICCAD)*, 2023, pp. 1–9.
- [12] T. Dao, D. Y. Fu, S. Ermon, A. Rudra, and C. Ré, “Flashattention: Fast and memory-efficient exact attention with io-awareness,” 2022. [Online]. Available: <https://arxiv.org/abs/2205.14135>
- [13] S. Dave, T. Nowatzki, and A. Shrivastava, “Explainable-dse: An agile and explainable exploration of efficient hw/sw codesigns of deep learning accelerators using bottleneck analysis,” in *Proceedings of the 28th ACM International Conference on Architectural Support for Programming Languages and Operating Systems, Volume 4*, ser. ASPLOS ’23. New York, NY, USA: Association for Computing Machinery, 2024, p. 87–107. [Online]. Available: <https://doi.org/10.1145/3623278.3624772>
- [14] G. F. de Oliveira Junior, M. Kabra, Y. Guo, K. Chen, A. G. Yaglikci, M. Soysal, M. Sadrosadati, J. O. Bueno, S. Ghose, J. Gómez-Luna, and O. Mutlu, “Proteus: Achieving high-performance processing-using-dram with dynamic bit-precision, adaptive data representation, and flexible arithmetic,” in *Proceedings of the 39th ACM International Conference on Supercomputing*, ser. ICS ’25. New York, NY, USA: Association for Computing Machinery, 2025, p. 473–494. [Online]. Available: <https://doi.org/10.1145/3721145.3730420>
- [15] Q. Deng, L. Jiang, Y. Zhang, M. Zhang, and J. Yang, “Dracc: a dram based accelerator for accurate cnn inference,” in *2018 55th ACM/ESDA/IEEE Design Automation Conference (DAC)*, 2018, pp. 1–6.
- [16] Q. Deng, Y. Zhang, M. Zhang, and J. Yang, “Lacc: Exploiting lookup table-based fast and accurate vector multiplication in dram-based cnn accelerator,” in *2019 56th ACM/IEEE Design Automation Conference (DAC)*, 2019, pp. 1–6.

[17] C. Eckert, X. Wang, J. Wang, A. Subramaniyan, R. Iyer, D. Sylvester, D. Blaauw, and R. Das, “Neural cache: Bit-serial in-cache acceleration of deep neural networks,” in *2018 ACM/IEEE 45th Annual International Symposium on Computer Architecture (ISCA)*, 2018, pp. 383–396.

[18] J. D. Ferreira, G. Falcao, J. Gómez-Luna, M. Alser, L. Orosa, M. Sadrosadati, J. S. Kim, G. F. Oliveira, T. Shahroodi, A. Nori, and O. Mutlu, “pluto: Enabling massively parallel computation in dram via lookup tables,” in *2022 55th IEEE/ACM International Symposium on Microarchitecture (MICRO)*, 2022, pp. 900–919.

[19] F. Gao, G. Tzantzioulis, and D. Wentzlaff, “Computedram: In-memory compute using off-the-shelf drams,” in *Proceedings of the 52nd Annual IEEE/ACM International Symposium on Microarchitecture*, ser. MICRO-52. New York, NY, USA: Association for Computing Machinery, 2019, p. 100–113. [Online]. Available: <https://doi.org/10.1145/3352460.3358260>

[20] N. Hajinazar, G. F. Oliveira, S. Gregorio, J. a. D. Ferreira, N. M. Ghiasi, M. Patel, M. Alser, S. Ghose, J. Gómez-Luna, and O. Mutlu, “Simdram: a framework for bit-serial SIMD processing using dram,” in *Proceedings of the 26th ACM International Conference on Architectural Support for Programming Languages and Operating Systems*, ser. ASPLOS ’21. New York, NY, USA: Association for Computing Machinery, 2021, p. 329–345. [Online]. Available: <https://doi.org/10.1145/3445814.3446749>

[21] T. J. Ham, B. K. Chelepalli, N. Xue, and B. C. Lee, “Disintegrated control for energy-efficient and heterogeneous memory systems,” in *2013 IEEE 19th International Symposium on High Performance Computer Architecture (HPCA)*, 2013, pp. 424–435.

[22] W. Han, H. Cho, D. Kim, and J.-Y. Kim, “Sal-pim: A subarray-level processing-in-memory architecture with lut-based linear interpolation for transformer-based text generation,” *IEEE Transactions on Computers*, vol. 74, no. 9, pp. 2909–2922, 2025.

[23] M. He, C. Song, I. Kim, C. Jeong, S. Kim, I. Park, M. Thottethodi, and T. N. Vijaykumar, “Newton: A dram-maker’s accelerator-in-memory (aim) architecture for machine learning,” in *2020 53rd Annual IEEE/ACM International Symposium on Microarchitecture (MICRO)*, 2020, pp. 372–385.

[24] K. Hegde, P.-A. Tsai, S. Huang, V. Chandra, A. Parashar, and C. W. Fletcher, “Mind mappings: enabling efficient algorithm-accelerator mapping space search,” in *Proceedings of the 26th ACM International Conference on Architectural Support for Programming Languages and Operating Systems*, ser. ASPLOS ’21. New York, NY, USA: Association for Computing Machinery, 2021, p. 943–958. [Online]. Available: <https://doi.org/10.1145/3445814.3446762>

[25] G. Heo, S. Lee, J. Cho, H. Choi, S. Lee, H. Ham, G. Kim, D. Mahajan, and J. Park, “Neupims: Npu-pim heterogeneous acceleration for batched llm inferencing,” in *Proceedings of the 29th ACM International Conference on Architectural Support for Programming Languages and Operating Systems, Volume 3*, ser. ASPLOS ’24. New York, NY, USA: Association for Computing Machinery, 2024, p. 722–737. [Online]. Available: <https://doi.org/ezproxy.lib.utexas.edu/10.1145/3620666.3651380>

[26] S. Hong, S. Moon, J. Kim, S. Lee, M. Kim, D. Lee, and J.-Y. Kim, “Dfx: A low-latency multi-fpga appliance for accelerating transformer-based text generation,” in *2022 IEEE Hot Chips 34 Symposium (HCS)*, 2022, pp. 1–17.

[27] M. Horeni, P. Taheri, P.-A. Tsai, A. Parashar, J. Emer, and S. Joshi, “Ruby: Improving hardware efficiency for tensor algebra accelerators through imperfect factorization,” in *2022 IEEE International Symposium on Performance Analysis of Systems and Software (ISPASS)*, 2022, pp. 254–266.

[28] Q. Huang, M. Kang, G. Dinh, T. Norell, A. Kalaiah, J. Demmel, J. Wawrzynek, and Y. S. Shao, “Cosa: scheduling by constrained optimization for spatial accelerators,” in *Proceedings of the 48th Annual International Symposium on Computer Architecture*, ser. ISCA ’21. IEEE Press, 2021, p. 554–566. [Online]. Available: <https://doi.org/10.1109/ISCA52012.2021.00050>

[29] W. Huang, H. Qin, Y. Liu, Y. Li, Q. Liu, X. Liu, L. Benini, M. Magno, S. Zhang, and X. Qi, “Slim-llm: Salience-driven mixed-precision quantization for large language models,” 2025. [Online]. Available: <https://arxiv.org/abs/2405.14917>

[30] J. Hyun, M. Seo, S. Jeong, H.-J. Lee, and X. T. Nguyen, “Dear-pim: Processing-in-memory architecture with disaggregated execution of all-bank requests,” in *2025 Design, Automation & Test in Europe Conference (DATE)*, 2025, pp. 1–7.

[31] Imec, “Technology platform for thermally stable dram peripheral transistors,” *Imec Magazine*, 2020, accessed: 2025-09-28. [Online]. Available: <https://www.imec-int.com/en/articles/technology-platform-thermally-stable-dram-peripheral-transistors>

[32] M. Isaev, N. McDonald, L. Dennison, and R. Vuduc, “Calculon: a methodology and tool for high-level co-design of systems and large language models,” in *Proceedings of the International Conference for High Performance*

Computing, Networking, Storage and Analysis, ser. SC '23. New York, NY, USA: Association for Computing Machinery, 2023. [Online]. Available: <https://doi.org/10.1145/3581784.3607102>

[33] B. Jacob, S. Ng, and D. Wang, *Memory Systems: Cache, DRAM, Disk*. San Francisco, CA, USA: Morgan Kaufmann Publishers Inc., 2007.

[34] Y. Jang, H. Cho, Y. Ryu, J. Kim, and S. Hong, "Pimpal: Accelerating llm inference on edge devices via in-dram arithmetic lookup," in *2025 62nd ACM/IEEE Design Automation Conference (DAC)*, 2025, pp. 1–7.

[35] A. Kahng, A. B. Kahng, H. Lee, and J. Li, "Probe: A placement, routing, back-end-of-line measurement utility," *IEEE Transactions on Computer-Aided Design of Integrated Circuits and Systems*, vol. 37, no. 7, pp. 1459–1472, 2018.

[36] A. B. Kahng and et al., "Probe2.0: A systematic framework for routability/beol co-optimization," *IEEE TCAD*, 2022.

[37] S.-C. Kao and T. Krishna, "Gamma: Automating the hw mapping of dnn models on accelerators via genetic algorithm," in *2020 IEEE/ACM International Conference On Computer Aided Design (ICCAD)*, 2020, pp. 1–9.

[38] S.-C. Kao, M. Pellauer, A. Parashar, and T. Krishna, "Digamma: domain-aware genetic algorithm for hw-mapping co-optimization for dnn accelerators," in *Proceedings of the 2022 Conference & Exhibition on Design, Automation & Test in Europe*, ser. DATE '22. Leuven, BEL: European Design and Automation Association, 2022, p. 232–237.

[39] J. S. Kim, M. Patel, H. Hassan, L. Orosa, and O. Mutlu, "D-range: Using commodity dram devices to generate true random numbers with low latency and high throughput," in *2019 IEEE International Symposium on High Performance Computer Architecture (HPCA)*, 2019, pp. 582–595.

[40] Y. Kim, R. Daly, J. Kim, C. Fallin, J. H. Lee, D. Lee, C. Wilkerson, K. Lai, and O. Mutlu, "Flipping bits in memory without accessing them: An experimental study of dram disturbance errors," in *2014 ACM/IEEE 41st International Symposium on Computer Architecture (ISCA)*, 2014, pp. 361–372.

[41] Y. Kim, V. Seshadri, D. Lee, J. Liu, and O. Mutlu, "A case for exploiting subarray-level parallelism (salp) in dram," *SIGARCH Comput. Archit. News*, vol. 40, no. 3, p. 368–379, Jun. 2012. [Online]. Available: <https://doi.org/10.1145/2366231.2337202>

[42] Y. Kim, W. Yang, and O. Mutlu, "Ramulator: A fast and extensible dram simulator," *IEEE Computer Architecture Letters*, vol. 15, no. 1, pp. 45–49, 2016.

[43] H. Kwon, A. Samajdar, and T. Krishna, "Maeri: Enabling flexible dataflow mapping over dnn accelerators via reconfigurable interconnects," *SIGPLAN Not.*, vol. 53, no. 2, p. 461–475, Mar. 2018. [Online]. Available: <https://doi.org/10.1145/3296957.3173176>

[44] W. Kwon, Z. Li, S. Zhuang, Y. Sheng, L. Zheng, C. H. Yu, J. E. Gonzalez, H. Zhang, and I. Stoica, "Efficient memory management for large language model serving with pagedattention," 2023. [Online]. Available: <https://arxiv.org/abs/2309.06180>

[45] Y. Kwon, K. Vladimir, N. Kim, W. Shin, J. Won, M. Lee, H. Joo, H. Choi, G. Kim, B. An, J. Kim, J. Lee, I. Kim, J. Park, C. Park, Y. Song, B. Yang, H. Lee, S. Kim, D. Kwon, S. Lee, K. Kim, S. Oh, J. Park, G. Hong, D. Ka, K. Hwang, J. Park, K. Kang, J. Kim, J. Jeon, M. Lee, M. Shin, M. Shin, J. Cha, C. Jung, K. Chang, C. Jeong, E. Lim, I. Park, J. Chun, and S. Hynix, "System architecture and software stack for gddr6-aim," in *2022 IEEE Hot Chips 34 Symposium (HCS)*, 2022, pp. 1–25.

[46] C. Lattner, M. Amini, U. Bondhugula, A. Cohen, A. Davis, J. Pienaar, R. Riddle, T. Shpeisman, N. Vasilache, and O. Zinenko, "Mlir: scaling compiler infrastructure for domain specific computation," in *Proceedings of the 2021 IEEE/ACM International Symposium on Code Generation and Optimization*, ser. CGO '21. IEEE Press, 2021, p. 2–14. [Online]. Available: <https://doi.org/10.1109/CGO51591.2021.9370308>

[47] C. Li, Y. Yin, X. Wu, J. Zhu, Z. Gao, D. Niu, Q. Wu, X. Si, Y. Xie, C. Zhang, and G. Sun, "H2-llm: Hardware-dataflow co-exploration for heterogeneous hybrid-bonding-based low-batch llm inference," in *Proceedings of the 52nd Annual International Symposium on Computer Architecture*, ser. ISCA '25. New York, NY, USA: Association for Computing Machinery, 2025, p. 194–210. [Online]. Available: <https://doi.org/10.1145/3695053.3731008>

[48] S. Li, A. O. Glova, X. Hu, P. Gu, D. Niu, K. T. Malladi, H. Zheng, B. Brennan, and Y. Xie, "Scope: A stochastic computing engine for dram-based in-situ accelerator," in *2018 51st Annual IEEE/ACM International Symposium on Microarchitecture (MICRO)*, 2018, pp. 696–709.

[49] S. Li, D. Niu, K. T. Malladi, H. Zheng, B. Brennan, and Y. Xie, "Drisa: A dram-based reconfigurable in-situ accelerator," in *2017 50th Annual IEEE/ACM International Symposium on Microarchitecture (MICRO)*, 2017, pp. 288–301.

[50] Z. Li, J. Zhou, X. Li, and N. Sun, “Blockpim: Optimizing memory management for pim-enabled long-context llm inference,” in *2025 62nd ACM/IEEE Design Automation Conference (DAC)*, 2025, pp. 1–7.

[51] C. Liu, D. Chen, Y. Huang, W. Xiao, H. Liu, Y. Zhang, H. Li, X. Liao, and H. Jin, “Seim: In-memory acceleration for approximate nearest neighbor search,” in *2025 62nd ACM/IEEE Design Automation Conference (DAC)*, 2025, pp. 1–7.

[52] J. Liu, M. Zhou, Y. Pan, C.-Y. Yang, L. Josipović, and T. Rosing, “Optipim: Optimizing processing-in-memory acceleration using integer linear programming,” in *Proceedings of the 52nd Annual International Symposium on Computer Architecture*, ser. ISCA ’25. New York, NY, USA: Association for Computing Machinery, 2025, p. 867–883. [Online]. Available: <https://doi.org.ezproxy.lib.utexas.edu/10.1145/3695053.3731041>

[53] M. Lokhande, G. Raut, and S. K. Vishvakarma, “Flex-pe: Flexible and simd multiprecision processing element for ai workloads,” *IEEE Transactions on Very Large Scale Integration (VLSI) Systems*, vol. 33, no. 6, pp. 1610–1623, 2025.

[54] L. Lu, N. Guan, Y. Wang, L. Jia, Z. Luo, J. Yin, J. Cong, and Y. Liang, “Tenet: A framework for modeling tensor dataflow based on relation-centric notation,” in *2021 ACM/IEEE 48th Annual International Symposium on Computer Architecture (ISCA)*, 2021, pp. 720–733.

[55] S. Ma, K. Mhatre, J. Weng, B. Hanindhito, Z. Wang, T. Nowatzki, L. John, and A. Arora, “Pimsab: A processing-in-memory system with spatially-aware communication and bit-serial-aware computation,” *ACM Trans. Archit. Code Optim.*, vol. 21, no. 4, Nov. 2024. [Online]. Available: <https://doi.org/10.1145/3690824>

[56] O. Naji, C. Weis, M. Jung, N. Wehn, and A. Hansson, “A high-level dram timing, power and area exploration tool,” in *2015 International Conference on Embedded Computer Systems: Architectures, Modeling, and Simulation (SAMOS)*, July 2015, pp. 149–156.

[57] W. Niu, G. Agrawal, and B. Ren, “Sod2: Statically optimizing dynamic deep neural network execution,” in *Proceedings of the 29th ACM International Conference on Architectural Support for Programming Languages and Operating Systems, Volume 1*, ser. ASPLOS ’24. New York, NY, USA: Association for Computing Machinery, 2024, p. 386–400. [Online]. Available: <https://doi.org/10.1145/3617232.3624869>

[58] NVIDIA, “Nvidia h100 tensor core gpu architecture,” <https://resources.nvidia.com/en-us-hopper-architecture/nvidia-h100-tensor-c>, 2025, accessed: 17 November 2025.

[59] G. F. Oliveira, A. Olgun, A. G. Yağlıkçı, F. N. Bostancı, J. Gómez-Luna, S. Ghose, and O. Mutlu, “Mimdram: An end-to-end processing-using-dram system for high-throughput, energy-efficient and programmer-transparent multiple-instruction multiple-data computing,” in *2024 IEEE International Symposium on High-Performance Computer Architecture (HPCA)*, 2024, pp. 186–203.

[60] A. Parashar, P. Raina, Y. S. Shao, Y.-H. Chen, V. A. Ying, A. Mukkara, R. Venkatesan, B. Khailany, S. W. Keckler, and J. Emer, “Timeloop: A systematic approach to dnn accelerator evaluation,” in *2019 IEEE International Symposium on Performance Analysis of Systems and Software (ISPASS)*, 2019, pp. 304–315.

[61] A. Paszke, S. Gross, F. Massa, A. Lerer, J. Bradbury, G. Chanan, T. Killeen, Z. Lin, N. Gimelshein, L. Antiga, A. Desmaison, A. Köpf, E. Yang, Z. DeVito, M. Raison, A. Tejani, S. Chilamkurthy, B. Steiner, L. Fang, J. Bai, and S. Chintala, *PyTorch: an imperative style, high-performance deep learning library*. Red Hook, NY, USA: Curran Associates Inc., 2019.

[62] A. Pathak, R. Balasubramonian, and N. Jouppi, “A modeling methodology for dram with 3d integration and heterogeneous technologies,” in *Proceedings of the Design, Automation and Test in Europe Conference (DATE)*. IEEE, 2013, pp. 1549–1554. [Online]. Available: <https://repository.lib.ncsu.edu/bitstreams/004e6091-4d63-41e7-9bc6-1d8a15cf3b22/download>

[63] X. Peng, Y. Wang, and M.-C. Yang, “Chopper: A compiler infrastructure for programmable bit-serial simd processing using memory in dram,” in *2023 IEEE International Symposium on High-Performance Computer Architecture (HPCA)*, 2023, pp. 1275–1288.

[64] R. Pope, S. Douglas, A. Chowdhery, J. Devlin, J. Bradbury, A. Levskaya, J. Heek, K. Xiao, S. Agrawal, and J. Dean, “Efficiently scaling transformer inference,” 2022. [Online]. Available: <https://arxiv.org/abs/2211.05102>

[65] L.-N. Pouchet, “Polybench: The polyhedral benchmark suite,” 2025, accessed on Nov 16, 2025. [Online]. Available: <https://www.cs.colostate.edu/~pouchet/software/polybench/>

[66] J. Ragan-Kelley, C. Barnes, A. Adams, S. Paris, F. Durand, and S. Amarasinghe, “Halide: a language and compiler for optimizing parallelism, locality, and recomputation in image processing pipelines,” in *Proceedings of the 34th ACM SIGPLAN Conference on Programming Language Design and Implementation*, ser. PLDI ’13. New York, NY, USA: Association for Computing Machinery, 2013, p. 519–530. [Online]. Available: <https://doi.org/10.1145/2491956.2462176>

[67] E. Russo, M. Palesi, G. Ascia, D. Patti, S. Monteleone, and V. Catania, “Memory-aware dnn algorithm-hardware mapping via integer linear programming,” in *Proceedings of the 20th ACM International Conference on Computing Frontiers*, ser. CF ’23. New York, NY, USA: Association for Computing Machinery, 2023, p. 134–143. [Online]. Available: <https://doi.org/10.1145/3587135.3592206>

[68] V. Seshadri, K. Hsieh, A. Boroum, D. Lee, M. A. Kozuch, O. Mutlu, P. B. Gibbons, and T. C. Mowry, “Fast bulk bitwise and and or in dram,” *IEEE Computer Architecture Letters*, vol. 14, no. 2, pp. 127–131, 2015.

[69] V. Seshadri, Y. Kim, C. Fallin, D. Lee, R. Ausavarungnirun, G. Pekhimenko, Y. Luo, O. Mutlu, P. B. Gibbons, M. A. Kozuch, and T. C. Mowry, “Rowclone: Fast and energy-efficient in-dram bulk data copy and initialization,” in *2013 46th Annual IEEE/ACM International Symposium on Microarchitecture (MICRO)*, 2013, pp. 185–197.

[70] V. Seshadri, D. Lee, T. Mullins, H. Hassan, A. Boroumand, J. Kim, M. A. Kozuch, O. Mutlu, P. B. Gibbons, and T. C. Mowry, “Ambit: In-memory accelerator for bulk bitwise operations using commodity dram technology,” in *2017 50th Annual IEEE/ACM International Symposium on Microarchitecture (MICRO)*, 2017, pp. 273–287.

[71] C. Silvano, D. Ielmini, F. Ferrandi, L. Fiorin, S. Curzel, L. Benini, F. Conti, A. Garofalo, C. Zambelli, E. Calore, S. Schifano, M. Palesi, G. Ascia, D. Patti, N. Petra, D. De Caro, L. Lavagno, T. Urso, V. Cardellini, G. C. Cardarilli, R. Birke, and S. Perri, “A survey on deep learning hardware accelerators for heterogeneous hpc platforms,” vol. 57, no. 11, Jun. 2025. [Online]. Available: <https://doi.org/10.1145/3729215>

[72] A. Spessot, T. Machleidt, C. Kenyon, and C.-H. Tsai, “Optimized material solutions for advanced dram,” *Physica Status Solidi (a)*, vol. 212, no. 1, pp. 47–53, 2015. [Online]. Available: <https://onlinelibrary.wiley.com/doi/10.1002/pssa.201532791>

[73] P. Spindler and F. M. Johannes, “Fast and accurate routing demand estimation for efficient routability-driven placement,” in *DATE*, 2007.

[74] E. Staff, “A new platform for thermally stable dram peripheral transistors,” *EDN Network*, 2018, accessed: 2025-09-28. [Online]. Available: <https://www.edn.com/a-new-platform-for-thermally-stable-dram-peripheral-transistors>

[75] J. E. Stine, I. Castellanos, M. Wood, J. Henson, F. Love, W. R. Davis, P. D. Franzon, M. Bucher, S. Basavarajaiah, J. Oh, and R. Jenkal, “Freepdk: An open-source variation-aware design kit,” in *2007 IEEE International Conference on Microelectronic Systems Education (MSE’07)*, 2007, pp. 173–174.

[76] Z. Tan, Z. Zhu, and K. Ma, “Cocco: Hardware-mapping co-exploration towards memory capacity-communication optimization,” in *Proceedings of the 29th ACM International Conference on Architectural Support for Programming Languages and Operating Systems, Volume 1*, ser. ASPLOS ’24. New York, NY, USA: Association for Computing Machinery, 2024, p. 69–84. [Online]. Available: <https://doi.org/10.1145/3617232.3624865>

[77] TechInsights. (2022) Industry-leading ddr5 technology: Micron vs. samsung. Accessed: 2025-10-02. [Online]. Available: <https://www.techinsights.com/blog/industry-leading-ddr5-technology>

[78] D. Thomas and P. Moorby, *The Verilog Hardware Description Language*, 5th ed. Springer Publishing Company, Incorporated, 2008.

[79] P. Tillet, H. T. Kung, and D. Cox, “Triton: an intermediate language and compiler for tiled neural network computations,” in *Proceedings of the 3rd ACM SIGPLAN International Workshop on Machine Learning and Programming Languages*, ser. MAPL 2019. New York, NY, USA: Association for Computing Machinery, 2019, p. 10–19. [Online]. Available: <https://doi.org/10.1145/3315508.3329973>

[80] N. Vasilache, O. Zinenko, T. Theodoridis, P. Goyal, Z. DeVito, W. S. Moses, S. Verdoolaege, A. Adams, and A. Cohen, “Tensor comprehensions: Framework-agnostic high-performance machine learning abstractions,” 2018. [Online]. Available: <https://arxiv.org/abs/1802.04730>

[81] J. Wang and J. Cong, “Search for optimal systolic arrays: A comprehensive automated exploration framework and lessons learned,” 2021. [Online]. Available: <https://arxiv.org/abs/2111.14252>

[82] K. Wang, K. Angstadt, C. Bo, N. Brunelle, E. Sadredini, I. Tracy, Tommy, J. Wadden, M. Stan, and K. Skadron, “An overview of micron’s automata processor,” in *Proceedings of the Eleventh IEEE/ACM/IFIP International Conference on Hardware/Software Codesign and System Synthesis*, ser. CODES ’16. New York, NY, USA: Association for Computing Machinery, 2016. [Online]. Available: <https://doi.org/10.1145/2968456.2976763>

[83] Y. N. Wu, P.-A. Tsai, A. Parashar, V. Sze, and J. S. Emer, “Sparseloop: An analytical approach to sparse tensor accelerator modeling,” in *Proceedings of the 55th Annual IEEE/ACM International Symposium on Microarchitecture*, ser. MICRO ’22. IEEE Press, 2023, p. 1377–1395. [Online]. Available: <https://doi.org/10.1109/MICRO56248.2022.00096>

[84] X. Xin, Y. Zhang, and J. Yang, “Elp2im: Efficient and low power bitwise operation processing in dram,” in *2020 IEEE International Symposium on High Performance Computer Architecture (HPCA)*, 2020, pp. 303–314.

[85] F.-L. Yang, C.-C. Huang, C.-C. Huang, T.-X. Chung, H.-Y. Chen, C.-Y. Chang, H.-W. Chen, D.-H. Lee, S.-D. Liu, K.-H. Chen, C.-K. Wen, S.-M. Cheng, C.-T. Yang, L.-W. Kung, C.-L. Lee, Y.-J. Chou, F.-J. Liang, L.-H. Shiu, J.-W. You, K.-C. Shu, B.-C. Chang, J.-J. Shin, C.-K. Chen, T.-S. Gau, P.-W. Wang, B.-W. Chan, P.-F. Hsu, J.-H. Shieh, S.-H. Fung, C. Diaz, C.-M. Wu, Y.-C. See, B. Lin, M.-S. Liang, J.-C. Sun, and C. Hu, “45nm node planar-soi technology with 0.296 /spl mu/m/sup 2/ 6t-sram cell,” in *Digest of Technical Papers. 2004 Symposium on VLSI Technology, 2004.*, 2004, pp. 8–9.

[86] X. Yang, M. Gao, Q. Liu, J. Setter, J. Pu, A. Nayak, S. Bell, K. Cao, H. Ha, P. Raina, C. Kozyrakis, and M. Horowitz, “Interstellar: Using halide’s scheduling language to analyze dnn accelerators,” in *Proceedings of the Twenty-Fifth International Conference on Architectural Support for Programming Languages and Operating Systems*, ser. ASPLOS ’20. New York, NY, USA: Association for Computing Machinery, 2020, p. 369–383. [Online]. Available: <https://doi.org/10.1145/3373376.3378514>

[87] H. Yu, H. Li, H. Shi, T. S. Huang, and G. Hua, “Any-precision deep neural networks,” 2021. [Online]. Available: <https://arxiv.org/abs/1911.07346>

[88] H. Zhang, A. Ning, R. B. Prabhakar, and D. Wentzlaff, “Llmcompass: Enabling efficient hardware design for large language model inference,” in *Proceedings of the 51st Annual International Symposium on Computer Architecture*, ser. ISCA ’24. IEEE Press, 2025, p. 1080–1096. [Online]. Available: <https://doi.org/10.1109/ISCA59077.2024.00082>

[89] M. Zhou, G. Chen, M. Imani, S. Gupta, W. Zhang, and T. Rosing, “Pim-dl: Boosting dnn inference on digital processing in-memory architectures via data layout optimizations,” in *2021 30th International Conference on Parallel Architectures and Compilation Techniques (PACT)*, 2021, pp. 1–1.

[90] R. Zhou, A. Roohi, D. Misra, and S. Angizi, “Flexidram: A flexible in-dram framework to enable parallel general-purpose computation,” ser. ISLPED ’22. New York, NY, USA: Association for Computing Machinery, 2022. [Online]. Available: <https://doi.org/10.1145/3531437.3539721>